

Energy Landscape of Zirconia Phase Transitions

Shu-Hui Guan, Xiao-Jie Zhang, and Zhi-Pan Liu*

Collaborative Innovation Center of Chemistry for Energy Material, Key Laboratory of Computational Physical Science (Ministry of Education), Shanghai Key Laboratory of Molecular Catalysis and Innovative Materials, Department of Chemistry, Fudan University, Shanghai 200433, China

S Supporting Information

ABSTRACT: The solid-phase transitions of zirconia are important phenomena for many industrial applications. Because of the lack of tools for resolving the atom displacement pattern, the transition kinetics has been disputed for over 60 years. Here, first-principles-based stochastic surface walking (SSW) pathway sampling is utilized for resolving the mechanism of ZrO_2 tetragonal-to-monoclinic solid-phase transition. Two types of lattice and atom correspondence allowed in phase transition are determined for the first time from energy criterion, which are originated from two nearly energy-degenerate lowest-transition pathways and one stress-induced ferroelastic transition channel of tetragonal phase. An orthorhombic crystal phase ($Pbc2_1$) is discovered to be a trapping state at low temperatures in phase transition, the presence of which does not create new orientation relation but deters transformation toughening significantly. This new finding may facilitate the design of new functional oxide materials in ceramic industry.

Zirconia is an important functional material, and the transformation between its different phases has great influence on the mechanical and physicochemical properties.¹ Among three common phases of ZrO_2 , the monoclinic phase (m phase) is the most stable at low temperatures (<1000 °C), whereas tetragonal (t phase) and cubic phases become more stable at high temperatures. The tetragonal-to-monoclinic (t - m) phase transformation, in particular, is widely exploited in mechanical ceramic toughening² and in heterogeneous catalysis for tuning surface activity³ because of the rapid and reversible transition above ~ 1000 °C and the appreciable volume increase (by 4.2%) with the coordination number of Zr decreasing from 8 to 7. Although it was long regarded as a prototype model of diffusionless Martensitic phase transition,^{4,5} the transformation kinetics at the atomic level is not established. To identify the pathway for solid-to-solid phase transition has been a general challenge in physics and material science.

For Martensitic phase transition, phenomenological theory outlines two critical conditions, i.e., the presence of (i) an orientation relation (OR) for lattice/atom correspondence and (ii) a strain-invariant plane, also known as a habit plane.^{6,7} In the past 60 years, different ORs for the t - m phase transition have been proposed, mainly on the basis of in situ X-ray diffraction and transmission electron microscopy observations.⁷⁻¹⁴ (For examples, see reviews by Kasatkin⁸ and Trolliard.)⁹ These ORs are also summarized in the Supporting Information. Importantly,

two ORs are most recognized in the literature: type C, $(100)_m // (110)_t$ and $[001]_m // [001]_t$ by Bailey,⁷ Bansal,¹⁰ and Smith,¹¹ and type B, $(100)_m // (110)_t$, $[010]_m // [001]_t$ by Patil,¹² Simeone,¹³ and Wu.¹⁴ (Here, the conventional tetragonal cell is utilized for the notation of surface and direction.) It is however unclear which OR is kinetically more favorable.⁹ In addition, the mechanism of the transition is further complexed by the finding of new transient phase in t - m phase transition, characterized as an orthorhombic phase (o phase) in recent theory and experiment studies.^{9,15} The structure of the o phase is still uncertain, and its role in the transition kinetics remains highly controversial.

Here, we utilize a novel theoretical tool, namely, stochastic surface walking (SSW) method for crystal sampling¹⁶⁻¹⁸ as integrated with density functional theory (DFT) calculations to sample exhaustively the phase space of ZrO_2 . The SSW sampling is able to capture the lattice and atom correspondence between phases directly from pathways on potential energy surface (PES). This approach in combination with quantum mechanics calculations can establish the energy function of phase transition without assuming any reaction coordinate and lattice/atom correspondence and thus differs from the phenomenological Landau-type theory where extensive group theory analysis is often required with assumed lattice correspondence.¹⁹

In SSW pathway sampling, we start from one single phase of ZrO_2 , defined as initial state (IS), and explore exhaustively its likely phases nearby (>2000 minima), defined as final state (FS), until a significant number of IS/FS pairs (>200) are collected. The pathway sampling was carried out using both 12- and 24-atom supercells in the framework of DFT calculations, which is essential to capture all the low-energy pathways. The simulations using two different supercells were found to produce the same lowest-energy pathways, implying that atoms are diffusionless in ZrO_2 phase transition. The variable-cell double-ended surface walking method¹⁶⁻¹⁸ is then utilized to locate the transition state (TS) explicitly between IS and FS, on the basis of which the low-energy pathways are determined by sorting the computed barriers. The TS of phase transition is defined as the saddle point with one and only one imaginary mode on PES that is spanned by the lattice and atom degrees of freedoms. All TSs are further confirmed by phonon frequencies calculations that are based on the density functional perturbation theory using a $(2 \times 2 \times 2)$ supercell (96-atom). All lowest-energy pathways were verified using total-energy plane-wave DFT method, where a kinetic energy cutoff of 500 eV and GGA-PBE functional²⁰ were utilized

Received: April 30, 2015

Published: June 15, 2015



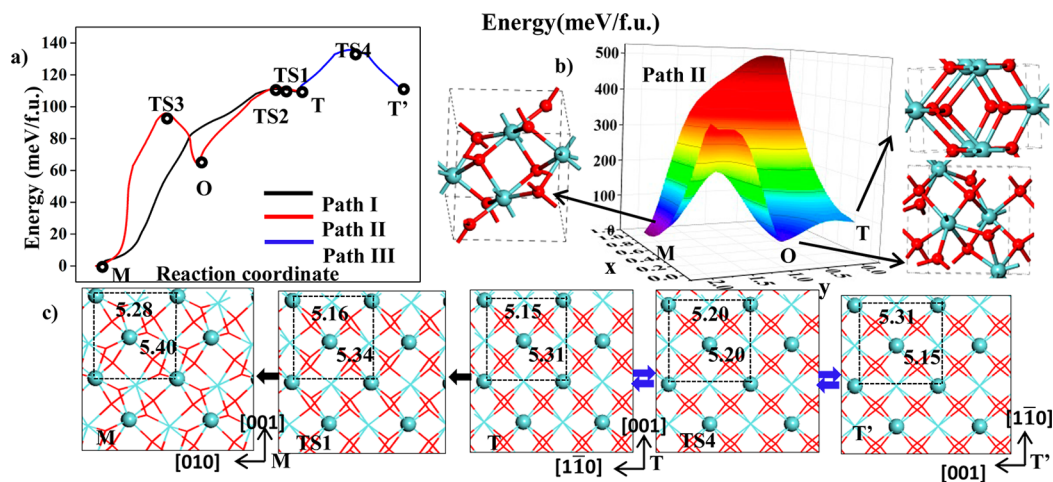


Figure 1. (a) Potential energy profile for the lowest energy pathways from tetragonal phase (T or T') to monoclinic (M) phase. (b) 3D PES of path II obtained by the linear interpolation of lattice parameters (x axis) and atomic fractional coordinates (y axis) from structure snapshots in path II. (c) Local structure change during phase transition following path I and III viewed down from the determined atomic habit plane, $(110)_t$ or $(100)_m$ surface. The Zr–Zr distances labeled are in Angstroms. Zr, cyan and O, red.

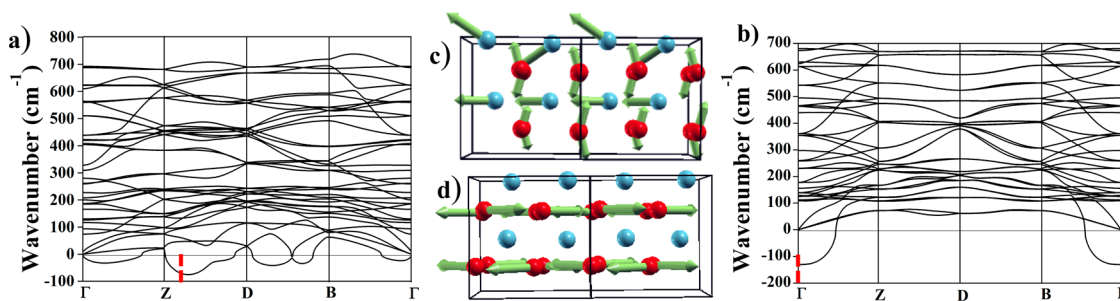


Figure 2. Calculated phonon dispersion for (a) TS1 and (b) TS4 and their associated imaginary phonon displacement eigenvector ((c) TS1 and (d) TS4). High-symmetry points of the Brillouin zone are denoted as Γ (0,0,0), Z (0,0,0.5), D (0.5,0,0.5), and B (0.5,0,0). The atomic movement vector is labeled using the green arrow. Zr, cyan and O, red.

to converge all values reported below 0.5 meV/f.u. (per ZrO_2 formula). The located low-energy pathways have been verified in large supercells up to 96-atoms. The hybrid DFT functional HSE06²¹ was also utilized to validate the energetics of all low-energy pathways, which yields a picture for the phase-transition mechanism consistent with that obtained using GGA-PBE functional. The other calculation details, including the DFT calculation setups, are described in Supporting Information.

From 269 pathways of t – m phase transition obtained from SSW sampling with 12- and 24-atom supercells (Supporting Information), we finally identify three distinct lowest-energy pathways. The overall potential energy profiles of these pathways are shown in Figure 1a. Paths I and II are pathways for t – m phase transition with the same apparent OR, i.e., $(100)_m // (110)_t$; $[001]_m // [001]_t$, which is the type-C OR in the literature. Unlike path I, path II is an indirect channel involving an intermediate orthorhombic phase, o phase $Pbc2_1$ (no. 29), with OR as $(100)_m // (001)_o$; $[001]_m // [100]_o$ and $(001)_o // (110)_t$; $[100]_o // [001]_t$. The 3D contour plot of path II is illustrated in Figure 1b. Path III is a branch channel involving the ferroelastic transformation of the t phase itself by switching the c and b axis. The OR is $(110)_t // (110)_t$; $[001]_t // [1\bar{1}0]_t$. When path III (t – t') is followed by path I or II (t – m), the apparent OR of t – m phase transition is changed to $(100)_m // (110)_t$; $[010]_m // [001]_t$, which turns out to be the type-B OR in the literature.

The calculated barriers (without considering the finite temperature effect) of paths I and II leaving t phase are

extremely low, 2.6 and 3.5 meV/f.u. relative to t phase, respectively, whereas that for path III is 29.2 meV/f.u., which is much higher than the previous two pathways. Compared to the t phase to o phase (t – o) transition, the o phase to m phase (o – m) transition in path II needs to overcome a much higher barrier (32.1 meV/f.u.), which indicates that the o phase is a trapping state at low temperatures. Because o phase is only 0.60% larger than t phase in volume, the transformation toughening is largely prevented because the o phase forms at low temperatures. Although the volume of o phase is close to that of t phase, the Zr in o phase is seven-coordinated and half of the O atoms are four-coordinated and the others are three-coordinated, which is the same as those in m phase. In short, in path II, the t – o phase transition breaks four Zr–O bonds per (12-atom) cell but with little change in the lattice; the o – m phase transition involves a large lattice distortion while keeping the overall coordination.

By closely inspecting these pathways, we can understand how atoms displace in phase transition. We illustrate in Figure 1c the atomic movement on $(110)_t$ and $(100)_m$ in paths I and III, where both types of OR can be generated. These surfaces are determined to be the atomic habit planes (interface) of the phases, which fulfill the following criteria: (i) minimum strain as evidenced by the close lattice parameters, e.g., $(110)_t = 5.15 \times 5.31 \text{ \AA}$ and $(100)_m = 5.28 \times 5.40 \text{ \AA}$ (Figure 1c), (ii) minimum atomic movement in phase transition, and (iii) a coherent interface achieved by close atomic match at the heterophase junction. Our theoretical procedure to identify the atomic habit

plane of phase transition is detailed in the Supporting Information.

Figure 2a depicts the phonon dispersions at the transition state (TS1) of path I, which plots along the path from Γ (0, 0, 0) to Z (0,0,0.5), Z–D (0.5,0,0.5), D–B (0.5,0,0), and B– Γ (0,0,0). By comparing the calculated phonon dispersions with the stable *t* phase and *m* phase where no imaginary phonon are present, we found that TS1 has an obvious imaginary phonon mode from Γ to Z and to D, which implies that the instability of the structure is due to the collective movement of atoms. The largest negative phonon mode (indicated by red lines) occurs in between the Z and D points, close to the high-symmetry Z point, which stiffens up rapidly away from the (0.15, 0, 0.5) point. Figure 2c also shows the corresponding displacement eigenvector of this imaginary mode. For the middle layer of Zr atoms, all vectors are polarized along the $[010]_m$ direction, parallel with the $(100)_m$ habit plane. The oxygen atom chains displace mainly perpendicular to the habit plane but also have relative slip parallel to the habit plane. Obviously, the structure instability at TS1 is caused mainly by the vibration of the Zr–O chains out of the habit plane, leading to the rearrangement of Zr coordination. (See also the Supporting Information for Zr coordination change.) We note that the main characteristics of phonon dispersion for TS2 and TS3 in path II are similar to those in TS1 and will not be discussed further.

Unlike the two lowest energy pathways, path III is not directly leading to *m* phase but is a ferroelastic transformation of *t* phase. Such a reorientation of the individual tetragonal domain is enabled by a permutation of the *b* and *c* axis in $(110)_t$ habit plane. The *t*–*t'* phase transition goes through TS4, which has a cubic-phase-like lattice ($P4/nbm$, no. 125). The diagonal Zr–Zr distances in the habit plane are all 5.20 Å (Figure 1c), giving rise to the volume drop at TS4 by 1.3%.

To understand the structural instability of TS4 in path III, we also analyzed its phonon dispersion and found that the imaginary mode of this ferroelastic phase transition TS which is different from other TSs is largely localized at the Γ point. Indeed, the atomic displacement of the imaginary mode relates entirely to the O atoms that displace relatively at the direction parallel to the habit plane, as shown in Figure 2d. It is the local O–Zr–O scissoring that leads to the compression of the lattice and eventually induces the ferroelastic transition. With the lowest energy pathways determined, we are now at the position to understand the phase transition kinetics that occur at phase transition temperatures. For this purpose, the free energies of the phases and the important intermediates along the pathways, including the TSs, were calculated by taking into account the zero-point energy and the phonon entropy contribution at the high temperatures. (See calculation detail in Supporting Information.) Figure 3 plots the variation of the free energy of the phases upon the change of temperature. Our theoretical calculations confirm that the *t* phase becomes more stable than the *m* phase above 1580 K, which is consistent with previous calculations (1560 K)²² and the experiment observation (1480–1550 K).^{23,24} (Transition temperature is reduced to 1450 K when hybrid HSE06 functional is utilized instead; Supporting Information)

Interestingly, we found that the stability of the intermediate *o* phase is very sensitive to temperature. It is more stable than the *t* phase below 800 K. Above 1000 K, *o* phase is no longer a stable phase (less stable than TS2 and *t* phase) and thus becomes an adaptive form in the transition pathway, dictating the highest energy position along path II. Consistent with our finding,

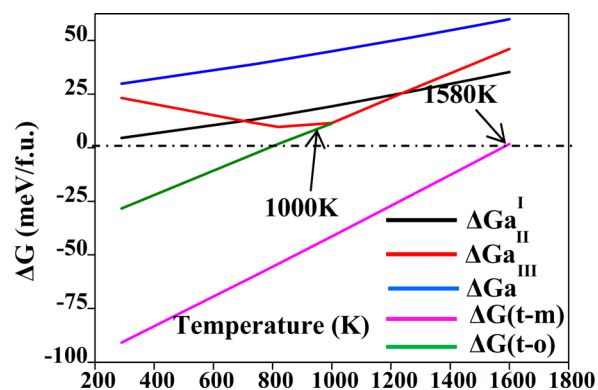


Figure 3. Gibbs free energies vs temperature diagram for ZrO₂ phase transition. ΔG , free energy difference between stable phases, ΔG_a , free energy barrier, $\Delta G_a^{\text{II}} = \max(\Delta G_a^{\text{II}}(t-o), \Delta G_a^{\text{II}}(o-m))$, being the effective barrier in path II.

Marshall et al. have shown that an *o* phase can be prepared by cooling the Mg partially stabilized ZrO₂ sample to 300 °C in experiment.²⁵ Fundamentally, this is caused by the structure features of *o* phase that are close to *m* phase. The phonon density of *o* phase is similar to that of *m* phase (Supporting Information Figure S4), and in particular, *o* phase has phonon density that is much less soft compared to that of *t* phase. Consequently, with the increase of temperature, *o* phase becomes less stable with respect to *t* phase, and above 1000 K, it is less stable than TS2, which is structurally close to *t* phase.

The temperature dependence of *t*–*m* transition kinetics can also be viewed from Figure 3. The free energy barrier of path I, the direct reaction channel, increases with the elevation of the temperature apparently because *t* phase is stabilized at high temperatures. The kinetics of path II is more complex because of the presence of the intermediate *o* phase, the stability of which is highly temperature sensitive. At the low temperatures, i.e., below 800 K, the kinetics of path II is limited by the higher barrier of the *o*–*t* phase transition, which becomes increasingly difficult with the decrease of the temperature. From theory, *o* phase at low temperatures is thus rather stable with high barriers leading to both *t* phase and *m* phase. By contrast, at the high temperatures, i.e., above 1000 K, *o* phase is an unstable form, and path II is reduced to a one-step phase transition process. Because the free energy barriers of paths I and II are very close (within 8 meV/f.u.) at ~1400 K, we expect that both pathways are present in the *t*–*m* reversible transition. The low *t*–*m* phase transition barrier agrees with the rapid Martensitic phase transition as utilized in ceramic transformation toughening.²⁶ We note that our barriers are significantly lower (by ~50 meV/f.u.) than the previous DFT calculation²⁷ with manually configured lattice/atom correspondence. This reflects that the reaction coordinate of solid phase transition is not intuitive and exhaustive pathway sampling is essential to reveal true lowest pathways.

From Figure 3, although it also varies upon the change of temperature, the *t*–*t'* ferroelastic phase transition is apparently more difficult than the other two pathways. This indicates that path III cannot compete with path I and II at typical temperatures and ambient pressure. From our results, type-B OR is likely only if the *t*–*t'* ferroelastic phase transition occurs before the *t*–*m* phase transition. Figure 3 therefore suggests that the OR of *t*–*m* phase transition should be dominated by type-C OR.¹⁰ Experimentally, type-B OR, although less often observed, was reported in the phase transition of high-temperature zirconia

single crystals²⁸ and in 3YSZ ceramics.¹⁴ It is natural to wonder whether type-B OR could ever be possible in t - m transition.

To resolve this puzzle, we have calculated the phase transition pathways under three different external pressures (hydrostatic) at 5, 7, and 10 GPa, which mimic the large stress-field that is developed at grain boundaries owing to the volume expansion during t - m phase transition. The results are summarized in Table 1. Among three pathways, we found that only path III is

Table 1. Calculated Enthalpy Change (meV/f.u.) for ZrO₂ Phase Transition under Different External Pressures (p)^a

p (GPa)	0	5	7	10
$\Delta H(t-m)$	-110.6	-65.7	-49.9	-29.4
$\Delta H(t-o)$	-44.4	-37.1	-33.2	-27.4
ΔH_a^I	2.6	18.6	27.6	41.8
ΔH_a^{II}	32.1	60.2	59.4	41.5
ΔH_a^{III}	29.2	17.5	14.8	13.1

^a ΔH and ΔH_a are defined similarly as those in Figure 3 caption for ΔG .

facilitated at high pressures, which turns out to be the lowest energy channel ($\Delta H_a^{III} = 17.5$ meV) at 5 GPa compared to other two pathways (18.6 and 60.2 meV). This is in fact not surprising because the cubic-phase-like TS4 has the smallest volume in all the located TSs and phases; thus, a compressive field helps to reduce the barrier greatly. (The volumes of TS1 and TS2 are larger than that of t phase, and that of TS3 is also larger than o phase.) We thus expect that under high pressure condition the type-B OR would be the more favorable OR for the t - m phase transition. We noticed that there is some experimental evidence that is consistent with this finding.^{29–31} For example, Chien et al.³⁰ utilizes Vickers microindentation experiment to induce the phase transition of Y-stabilized ZrO₂ from t phase to m phase. They observe the ferroelastic domain switching of t phase together with the t - m Martensitic transition, and importantly, only type-B OR is found in the experiment. We emphasize that the presence of o phase does not add new OR.⁹ An important implication from current theoretical sampling on PES of ZrO₂ is that multiple nearly energy-degenerate reaction channels can coexist in solid-to-solid phase transition and share the same OR. The knowledge of OR that is possible to obtain from experiment is in fact not enough to resolve the mechanism and kinetics of solid phase transition.

We determine the structure of transient phase and resolve the physical origin of two types of OR in ZrO₂ t - m phase transition. We show via automated energy landscape sampling with new theoretical tools that the lowest energy pathways connecting crystal phases can now be mapped out to clarify the solid-to-solid phase transition mechanism and kinetics. The atomic structures in phase transition and at heterophase junction provide a quantitative basis for subsequent investigations on designing new materials with desirable mechanics and physicochemical properties.

■ ASSOCIATED CONTENT

📄 Supporting Information

OR from literature; SSW methodology and methods to determine atomic habit plane; and XYZ coordinate of pathways. The Supporting Information is available free of charge on the ACS Publications website at DOI: 10.1021/jacs.5b04528.

■ AUTHOR INFORMATION

Corresponding Author

*zpliu@fudan.edu.cn

Notes

The authors declare no competing financial interest.

■ ACKNOWLEDGMENTS

This work is supported by National Science Foundation of China (21173051, 21361130019), 973 program (2011CB808500, 2013CB834603), Science and Technology Commission of Shanghai Municipality (08DZ2270500), and Program for Professor of Special Appointment (Eastern Scholar) at Shanghai Institute of Higher Learning.

■ REFERENCES

- (1) Kelly, P. M.; Rose, L. R. *F. Prog. Mater. Sci.* **2002**, *47*, 463–557.
- (2) Jin, X.-J. *Curr. Opin. Solid State Mater. Sci.* **2005**, *9*, 313–318.
- (3) Wang, C. M.; Fan, K. N.; Liu, Z. P. *J. Am. Chem. Soc.* **2007**, *129*, 2642–2647.
- (4) Bhattacharya, K.; Conti, S.; Zanzotto, G.; Zimmer, J. *Nature* **2004**, *428*, 55–59.
- (5) Wolten, G. M. *J. Am. Ceram. Soc.* **1963**, *46*, 418–422.
- (6) Levitas, V.; Idesman, A.; Preston, D. *Phys. Rev. Lett.* **2004**, *93*, 105701–105704.
- (7) Bailey, J. E. *Proc. R. Soc. London, Ser. A* **1964**, *279*, 395–412.
- (8) Kasatkina, I.; Girgadiesa, F.; Ressler, T.; Carusoc, R. A.; Schattkac, J. H.; Urbana, J.; Weissa, K. *J. Mater. Sci.* **2004**, *39*, 2151–2157.
- (9) Troliard, G.; Mercurio, D.; Perez-Mato, J. M. *Z. Kristallogr.* **2011**, *226*, 264–290.
- (10) Bansal, G. K.; Heuer, A. H. *Acta Metall.* **1974**, *22*, 409–417.
- (11) Smith, D. K.; Newkirk, W. *Acta Crystallogr.* **1965**, *18*, 983–991.
- (12) Patil, R. N.; Subbarao, E. C. *Acta Crystallogr., Sect. A* **1970**, *26*, 535–541.
- (13) Simeone, D.; Baldinozzi, G.; Gosset, D.; Dutheil, M.; Bulou, A.; Hansen, T. *Phys. Rev. B* **2003**, *67*, 064111–064118.
- (14) Wu, Y.-C.; Chiang, Y.-T. *J. Am. Ceram. Soc.* **2011**, *94*, 2200–2212.
- (15) Liu, S.; Hu, W.; Zhang, Y.; Xiang, J.; Wen, F.; Xu, B.; He, J.; Yu, D.; Tian, Y.; Liu, Z. *J. Appl. Crystallogr.* **2014**, *47*, 684–691.
- (16) Shang, C.; Liu, Z. P. *J. Chem. Theory Comput* **2013**, *9*, 1838–1845.
- (17) Zhang, X. J.; Shang, C.; Liu, Z. P. *J. Chem. Theory Comput* **2013**, *9*, 3252–3260.
- (18) Shang, C.; Zhang, X. J.; Liu, Z. P. *Phys. Chem. Chem. Phys.* **2014**, *16*, 17845–17856.
- (19) Smirnov, M.; Mirgorodsky, A.; Guinebreteiere, R. *Phys. Rev. B* **2003**, *68*, 104106–104116.
- (20) Perdew, J. P.; Burke, K.; Ernzerhof, M. *Phys. Rev. Lett.* **1996**, *77*, 3865–3868.
- (21) Krukau, A. V.; Vydrov, O. A.; Izmaylov, A. F.; Scuseria, G. E. *J. Chem. Phys.* **2006**, *125*, 224106–224111.
- (22) Sternik, M.; Parlinski, K. *J. Chem. Phys.* **2005**, *122*, 064707–064713.
- (23) Ricca, C.; Ringuede, A.; Cassir, M.; Adamo, C.; Labat, F. *J. Comput. Chem.* **2015**, *36*, 9–21.
- (24) Frey, F.; Boysen, H.; Vogt, T. *Acta Crystallogr., Sect. B* **1990**, *46*, 724–730.
- (25) Marshall, D. B.; Jarnes, M. R.; Porter, J. R. *J. Am. Ceram. Soc.* **1989**, *72*, 218–227.
- (26) Bocanegra-Bernal, M. H.; Torre, S. D. D. I. *J. Mater. Sci.* **2002**, *37*, 4947–4971.
- (27) Luo, X.; Zhou, W.; Ushakov, S.; Navrotsky, A.; Demkov, A. *Phys. Rev. B* **2009**, *80*, 134119–134132.
- (28) Wolten, G. M. *Acta Crystallogr.* **1964**, *17*, 763–765.
- (29) Cain, M. G.; Lewis, M. H. *Mater. Lett.* **1990**, *9*, 309–312.
- (30) Chien, F. R.; Ubc, F. j.; Prakash, V.; Heuer, A. H. *Acta Mater.* **1998**, *46*, 2151–2171.
- (31) Lenz, L. K.; Heuer, A. H. *Commun. Am. Ceram. Soc.* **1982**, C192–C194.